Photoenhanced sulfates formation by the heterogeneous uptake of SO_2 on non-photoactive mineral dust

Wangjin Yang, Jiawei Ma, Hongxing Yang, Fu Li, Chong Han*

School of Metallurgy, Northeastern University, Shenyang, 110819, China

*Address correspondence to author: hanch@smm.neu.edu.cn

Short summary. We provide direct evidences that light prominently enhances the conversion of SO_2 to sulfates on non-photoactive mineral dust, where triplet states of SO_2 ($^3SO_2$) can act as a pivotal trigger to generate sulfates. Photochemical sulfate formation depends on H_2O, O_2, and basicity of mineral dust. It is suggested that the SO_2 photochemistry on non-photoactive mineral dust significantly contributes to sulfates, highlighting previously unknown pathway to better explain the missing sources of atmospheric sulfates.

Abstract. Heterogeneous uptake of SO_2 on mineral dust is a predominant formation pathway of sulfates, whereas the contribution of photo-induced SO_2 oxidation to sulfates on the dust interfaces still remains unclear. Here, we investigated heterogeneous photochemical reactions of SO_2 on five mineral oxides (SiO_2, kaolinite, Al_2O_3, MgO, and CaO) without photocatalytic activity. Light significantly enhanced the uptake of SO_2, and its enhancement effects negatively depended on the basicity of mineral oxides. The initial uptake coefficient ($\gamma_{0,\,BET}$) and the steady-state uptake coefficient ($\gamma_{s,\,BET}$) of SO_2 positively relied on light intensity, relative humidity (RH) and O_2 content, while they exhibited a negative relationship with the initial SO_2 concentration. Rapid sulfate formation during photo-induced heterogeneous reactions of SO_2 with all mineral oxides was confirmed to be ubiquitous, and H_2O and O_2 played the key roles in the conversion of SO_2 to sulfates. Specially, triplet states of SO_2 ($^3SO_2$) was suggested to be the trigger for photochemical sulfate formation. Atmospheric implications supported a potential contribution of interfacial SO_2 photochemistry on non-photoactive mineral dust to atmospheric sulfate sources.

Keywords: SO_2; Sulfates; Non-photoactive mineral dust; Heterogeneous photochemistry

1 Introduction

As an important trace gas in the atmosphere, SO_2 is mainly emitted by volcanic eruption and fuel combustion. There is an uneven distribution of atmospheric SO_2 concentrations that show a distinctive seasonal and regional differentiation. Typical ratios of SO_2 in the troposphere are below 0.5 ppb for a clean weather in remote areas, rising to around several hundred ppb during the polluted days in urban regions (Ma et al., 2020). About half of SO_2 is oxidized to sulfates (He et al., 2012), which is one of the most significant compositions in fine particles. The mass fraction of sulfates in $PM_{2.5}$ is high up to 30% (Shao et al., 2019), especially in polluted regions where high-sulfur fuels are usually used (Olson et al., 2021). They significantly alter physicochemical properties of aerosols in terms of hygroscopicity, acidity and light absorption property (Chan and Chan, 2003; Cao et al., 2013; Lim et al., 2018). Sulfates also pose a human health risk through causing respiratory illness and cardiovascular (Shiraiwa et al., 2017). In addition, the deposition of sulfates leads to adverse effects on ecosystems via the acidification of soils and lakes (Golobokova et al., 2020). Therefore, the oxidation of SO_2 to form sulfates has attracted widespread attention in the past decades.

The conversion of SO_2 to sulfates in the atmosphere usually occurs in different phases: gas-phase oxidation of SO_2 by hydroxyl radicals (•OH) or Criegee intermediate radicals (Mauldin et al., 2012; Davis et al., 1979); aqueous-phase reaction of SO_2 with O_3, peroxides or transition metal ions dissolved in cloud and fog droplets (Alexander et al., 2009; Herrmann et al., 2000; Harris et al., 2013; Liu et al., 2020a; Li et al., 2020); and heterogeneous SO_2 uptake on aerosols including authentic mineral dust, soot, inorganic ion and organic compounds (Adams et al., 2005; He et al., 2018a; Ye et al., 2018; Wang et al., 2019; Yao et al., 2019; Zhang et al., 2020a; Liu et al., 2020; Liu et al., 2021). However, the oxidation of SO_2 in gas and aqueous phases fails to explain high sulfate concentrations under polluted conditions. Model simulation

suggests that the rapid sulfate formation can be attributed to the heterogeneous SO_2 uptake (Li et al., 2017). A positive relationship between the fraction of sulfates and mineral dust in haze days has been reported, implying that mineral dust may account for the formation of sulfates (Wang et al., 2020a). Moreover, a large amount of sulfates was observed to be formed on the surface of mineral dust after long-distance transport (Prospero, 1999). Thus, investigating the heterogeneous oxidation of SO_2 on mineral dust can provide basic data for the model calculation to evaluate atmospheric sulfates.

Mineral dust, regarded as the dominant component of particulate matters in the atmosphere, accounts for about 30%−60% mass fractions of global aerosols (Dentener et al., 1996; Peng et al., 2012). It primarily contains SiO_2 (40%−80%), followed by Al_2O_3 (10%−15%), Fe_2O_3 (6%−13%), CaO (3%−10%), MgO (1%−7%) and TiO_2 (0.1%−5%) (Urupina et al., 2021; Urupina et al., 2019; Usher et al., 2003). Mineral dust can provide active sites for adsorption and reaction of gases. Up to now, the heterogeneous SO_2 uptake on authentic mineral aerosols and model mineral oxides has been widely reported (Ma et al., 2019; Goodman et al., 2001; Wang et al., 2018; Wang et al., 2020b), with various uptake coefficients (γ) of SO_2 varying from 10^{-9} to 10^{-4} (Urupina et al., 2019; Usher et al., 2002).

It was recognized that light could significantly enhance heterogeneous conversion of SO_2 to sulfates on the surface of photocatalytic mineral dust (Chen et al., 2021; Li et al., 2019; Wang et al., 2020b). Electron-hole pairs are produced via photo-induced electrons from the valence band to the conduction band of photocatalytic metal oxides, and then react with H_2O and O_2 to generate reactive oxygen species (ROS), such as •OH and $\bullet O_2^-$ (Chu et al., 2019). Sulfates are produced by the heterogeneous reactions of SO_2 with ROS (Park and Jang, 2016; Park et al., 2017; Langhammer et al., 2020; Bounechada et al., 2017). In particular, due to the large abundance of non-photoactive mineral dust (more than 85% mass of total mineral dust in the atmosphere) (Usher et al., 2003; Liu et al., 2022), revealing the photooxidation processes of SO_2 on these mineral dust is of great importance to better reevaluate the sulfate formation on aerosols in the global scale.

Hence, photochemical SO_2 uptake and sulfate formation on non-photoactive mineral oxides

were firstly investigated using a flow reactor and an *in situ* diffuse reflectance infrared Fourier transform spectroscopy (DRIFTS). The SO_2 conversion to sulfates was examined under various conditions, and the roles of light intensity, SO_2 concentration, H_2O, O_2 and basicity of mineral oxides were determined. Reaction mechanisms and atmospheric implications were proposed, highlighting a new and important pathway accounting for photochemical uptake of SO_2 to form sulfates on the non-photoactive surfaces.

2 Experimental methods

2.1 Materials

Analytical grade SiO_2 (Sinopharm Chemical Reagent Co., Ltd.), kaolinite (Sinopharm Chemical Reagent Co., Ltd.), Al_2O_3 (Alfa Aesar), MgO (Sigma-Aldrich), and CaO (Sigma-Aldrich) were used in the experiments. Through the nitrogen Brunauer-Emmett-Teller (BET) physisorption analysis, their specific surface areas were detected to be 0.419, 6.407, 8.137, 10.948 and 6.944 $m^2\ g^{-1}$, respectively. With $BaSO_4$ used as the reference, the ultraviolet-visible (UV-vis) light absorption spectra of samples (Figure S1) in the wavelength range of 300–800 nm were obtained by the Shimadzu UV-2550 spectrophotometer, which was equipped with diffuse reflection integrating sphere attachment. The solid powder (0.2−5 g) was uniformly dispersed into 10.0 mL ethanol solution. The mixed liquid was poured into a rectangle quartz sample dish (14.0 cm × 7.0 cm) and dried to form a solid coating in an oven at 353 K for 10 h. SO_2 standard gas (50 ppm in N_2, Shenyang Air Liquide Co., LTD) and high purity N_2 and O_2 (99.999 vol.%, Shenyang Air Liquide Co., LTD) were used as received. The solid sample powder (0.2 g) was immersed into 10 mL deionized water (20 mg mL^{-1}), and then the suspension was vigorously stirred for 10 min. The pH of SiO_2, kaolinite, Al_2O_3, MgO and CaO suspension was measured to be 6.27, 6.58, 9.33, 10.61 and 12.72 using a pH meter, respectively, which was employed to characterize the basicity of mineral oxides.

2.2 Rectangular flow reactor

The uptake experiments of SO_2 on mineral dust were performed in a horizontal rectangular flow reactor (26.0 cm length × 7.5 cm width × 2.0 cm height), which was depicted in Figure

S2. In a previous study, a similar rectangular flow reactor was designed and the feasibility of the reactor has been verified (Knopf et al., 2007). The reactor was made of quartz to allow the transmission of light. The temperature was maintained at 298 K by circulating temperature-controlled water through the outer jacket of the reactor. Synthetic air with a N_2/O_2 volume ratio of 4:1 was introduced into the flow reactor, and its total flow rate was 1000 mL min^{-1}. The Reynolds number (*Re*) was calculated to be 28.2 (*Re* < 200), as described in the Supporting Information, indicating a laminar flow state. SO_2 with high purity N_2 (100 mL min^{-1}) as carrier gas were introduced into the reactor through a movable T-shaped injector equipped with six exit holes of 0.2 mm diameter, so that the gas could be uniformly distributed over the width of the reactor. The SO_2 concentration was 40−200 ppb and measured with a SO_2 analyzer (Thermo 43i). Wet N_2 generated with a bubbler containing deionized water was introduced by two parallel inlets on the side of T-shaped injector. Relative humidity (RH, 10%−75%) was controlled by regulating the ratio of dry N_2 to wet N_2 and measured via a hygrometer (Center 314). The equivalent layer numbers of water on surface was 0.9−4.0 according to the Brunauer-Emmett-Teller (BET) model (Sumner et al., 2004), and the thickness of the film of adsorbed water varied between 2.7−12 nm at RH=10%−75%. There were three equally spaced exhaust ports to mitigate the outlet turbulence. A xenon lamp (CEL-LAX500, China Education Au-light Co., Ltd) was used to simulate sunlight and vertically located above the reactor. A filter was placed on the reactor to remove the light with wavelengths shorter than 300 nm. The spectrum irradiance of the xenon lamp was displayed in Figure S3 and measured using a calibrated spectroradiometer (ULS2048CL-EVO, Avantes). The spectral irradiance was measured inside the reactor, after passing the water cooling and in the absence of a sample. The total irradiance (0−7.93 × 10^{16} photons cm^{-2} s^{-1}) on the coating can be adjusted by varying the distance of the xenon lamp to the reactor.

2.3 Uptake coefficient of SO_2

The heterogeneous reaction kinetics of SO_2 with mineral dust can be described by a pseudo-first-order reaction. SiO_2 was taken as an example, and Figure S4 showed a linear relationship between the natural logarithm of the SO_2 concentration and the reaction time. The apparent rate

constant ($k_{obs,\ SiO_2}$) of SO_2 with SiO_2 can be calculated using the equation 1,

$$\frac{\ln(C_0/C_t)}{t} = k_{obs,\ SiO_2} \quad (1)$$

where C_0 and C_t (ppb) are the initial SO_2 concentration and the SO_2 concentration, respectively; t was calculated by diving the length of the reactive surface by the average flow velocity. The loss of SO_2 on the internal wall of the reactor in blank experiments was carried out under various conditions (Figure S5 as an example), and it has been deducted for the γ calculation. Assuming that the wall loss was constant in the experiments with and without samples, the geometric uptake coefficient (γ_{geo}) was determined by the equation 2 (Knopf et al., 2007),

$$\gamma_{geo} = \frac{4Vk}{S\omega} \quad (2)$$

where k (s^{-1}), V (4×10^{-4} m^3), S (9.8×10^{-3} m^2) and ω (314.05 m s^{-1}) are the reaction rate constant, the volume of the rectangular reactor, the surface area of the sample dish, and the mean molecular speed of SO_2, respectively.

The uptake process of SO_2 on SiO_2 depended on the reaction of SO_2 with SiO_2 and the mass transport of SO_2 to the surface. It can be expressed with the equation 3,

$$k'_{r,\ SiO_2} = \left[\frac{1}{k_{obs,\ SiO_2} - k_{obs,\ wall}} - \frac{a}{N_u D}\right]^{-1} \quad (3)$$

where $k_{obs,\ SiO_2}$ and $k_{obs,\ wall}$ (s^{-1}) are the apparent rate constants measured with and without SiO_2 samples, respectively. $k'_{r,\ SiO_2}$ is the reaction rate constant of SO_2 accounting for the diffusion effect; D (0.1337 cm^2 s^{-1}) is the diffusion coefficient of SO_2 in air; a (1 cm) is one half height of the flow reactor; N_u is the Nusselt numbers obtained with a calculation method from Solbrig and Gidaspow (1967), which represents the mass transport. Then, the corrected γ can be calculated by the equation 2 where k was replaced by $k'_{r,\ SiO_2}$. In our experiments, the correction for γ was estimated to be approximate 10%. Initial uptake coefficients (γ_0) and steady-state uptake coefficients (γ_s) were calculated by averaging the signals within the 1.0 and 40−60 min reaction time, respectively.

To understand the diffusion depth of SO_2 and determine the interaction of SO_2 with the underlying layers of SiO_2, the uptake of SO_2 as a function of the SiO_2 mass under irradiation

was shown in Figure S6. The γ exhibited a linear increase in the SiO_2 mass range of 0.05−2.0 g, while it remained unchanged at the SiO_2 mass > 3.0 g. Therefore, the uptake coefficient of SO_2 in the linear regions was normalized using the BET surface area of SiO_2 by the equation 4 (Brunauer et al., 1938),

$$\gamma_{BET}=\frac{S_{geo}\times\gamma_{geo}}{S_{BET}\times m_{SiO_2}} \quad (4)$$

where γ_{BET} is the SO_2 uptake coefficient normalized to the BET surface area; S_{geo} (9.8×10^{-3} m^2) is the geometric area of the sample dish; S_{BET} (0.419 m^2 g^{-1}) is the BET surface area of SiO_2; m_{SiO_2} (0.05−2.0 g) is the SiO_2 mass. The same method was also used to calculate the uptake coefficients of SO_2 on other mineral oxides.

2.4 In Situ DRIFTS analysis

The changes in the chemical compositions on mineral oxides in the SO_2 uptake process were investigated by the Fourier transform infrared (FTIR) spectrometer (Thermo Nicolet iS50) equipped with an *in situ* diffuse reflectance accessory and a mercury cadmium telluride (MCT) detector. About 14 mg mineral oxides was placed into a stainless-steel cup inside the reaction cell. To remove adsorbed impurities, SiO_2 was purged with a 150 mL min^{-1} airflow (N_2/O_2 volume ratio = 4:1) at RH=40% for 1 h. Then, a background spectrum of unreacted samples was collected. SO_2 (2 ppm) was introduced into the reaction cell, and the IR spectra was recorded as a function of time at a resolution of 4 cm^{-1} by averaging 100 scans. The light from the xenon lamp (500 W) was transmitted into the DRIFTS reaction cell via a fiber. To verify the role of intermediate, $Ru(bpy)_3(Cl)_2$) and $NaHCO_3$, acting as $^3SO_2$ and •OH scavengers (Bulgakov and Safonova, 1996; Gen et al., 2019a), respectively, were mixed with SiO_2 powder in an agate mortar, and the mixture was put in the reaction cell of DRIFTS.

3 Results and discussion

3.1 Photo-enhanced uptake of SO_2

Acting as the most abundant mineral oxides, SiO_2 was firstly used to investigate the uptake behaviors of SO_2. As shown in Figure 1A, when SO_2 (80 ppb) was exposed to SiO_2 in the dark,

193 the SO_2 concentration decreased to 70 ppb, and then it quickly increased and reached the steady
194 state after 20 min. Upon exposure to SiO_2 under irradiation, the SO_2 concentration exhibited a
195 greater drop than that in the dark. The deactivation of SO_2 uptake on SiO_2 was very slight after
196 20 mins under irradiation. These suggest that light can significantly promote the heterogeneous
197 reaction of SO_2 on SiO_2. When SO_2 did not contact with SiO_2, its concentration recovered
198 rapidly. The desorption of SO_2 was observed when SO_2 was isolated from SiO_2 in the dark and
199 under irradiation, indicating that the physical adsorption partially contributed to the SO_2 loss
200 during the photochemical process. The proportion of the desorbed SO_2 during the uptake
201 process can be quantified by dividing the integral of reversible desorption of SO_2 (t = 80–100
202 min) into the integral of the SO_2 uptake (t = 20–80 min), which was calculated to be 95% and
203 12% in the dark and under irradiation, respectively. This implies that SO_2 uptake in the dark
204 was primarily ascribed to the physical adsorption of SO_2, while SO_2 uptake under irradiation
205 was mainly attributed to chemical processes or irreversible adsorption.
206 The uptake coefficients of SO_2 on SiO_2 as a function of irradiation intensity were shown in
207 Figure 1B. The errors in all figures are the standard deviations of three repetitive experiments.
208 Both $\gamma_{0,\,BET}$ and $\gamma_{s,\,BET}$ displayed a well linear relationship with the irradiation intensity, further
209 confirming the photochemical nature for the reactions of SO_2 on SiO_2. In particular, $\gamma_{0,\,BET}$ and
210 $\gamma_{s,\,BET}$ on SiO_2 under simulated solar irradiation was comparable with those (10^{-7}–10^{-6}) on
211 Gobi Desert dust (GDD) and Arizona Test Dust (ATD) under UV irradiation, which contained
212 photocatalytic metal oxides (Park et al., 2017). As for the SO_2 uptake on TiO_2, $\gamma_{0,\,BET}$ and $\gamma_{s,\,BET}$
213 were measured to be 10^{-6} and 10^{-7}, respectively, by using the flow tube (Ma et al., 2019), which
214 were similar to our results. It should be pointed out that the similar uptake coefficient did not
215 mean the comparable ability of photoactive and non-photoactive mineral oxides to SO_2 uptake,
216 since the uptake coefficient was highly dependent on environmental conditions (SO_2
217 concentration, relative humidity, mineral oxides mass, light source and pressure) and reactor
218 type (chamber and flow tube reactor), and the uptake coefficients mentioned here were not
219 obtained under the exact same reaction conditions used in our study. The purities of different

mineral substances are 95%–98%. If photoactive impurities mainly contributed to the SO_2 uptake in the experiment, the SO_2 uptake coefficient on impurities should be 20–50 times higher than the current SO_2 uptake coefficient and range from 10^{-5} to 10^{-3}. The SO_2 uptake coefficient on photoactive substances was reported to be 10^{-7}–10^{-6} in previous studies (Ma et al., 2019; Park et al., 2017). Thus, the impurities in minerals were less likely responsible for the SO_2 uptake.

Figure 1C shows the evolution of $\gamma_{0,\,BET}$ and $\gamma_{s,\,BET}$ at different SO_2 concentrations under irradiation. An inverse dependence of $\gamma_{0,\,BET}$ and $\gamma_{s,\,BET}$ on the SO_2 concentration was observed, meaning that both initial and steady-state uptake reactions were lower efficient at higher SO_2 concentrations. The uptake of gases on the solid surfaces usually follows the Langmuir-Hinshelwood (L-H) mechanism (Ammann et al., 2003; Zhang et al., 2020b), suggesting that gaseous molecules are quickly absorbed on the surfaces, and then the reactions occur among the absorbed species. Assuming that the adsorption of SO_2 on SiO_2 is in accord with the Langmuir isotherm, the dependence of γ on the SO_2 concentration can be described by the equation 5 (Zhang et al., 2020b),

$$\gamma=\frac{(4V/S\omega)k[SiO_2]_T K_{SO_2}}{1+K_{SO_2}[SO_2]_g} \quad (5)$$

where $[SO_2]_g$ is the concentration of gaseous SO_2; $[SiO_2]_T$ is the total number of active sites on SiO_2; k is the reaction rate constant of SO_2 absorbed on SiO_2; K_{SO_2} represents the Langmuir adsorption constant of SO_2. Because the SiO_2 mass remained constant during the reaction, the equation 5 can be written as the equation 6,

$$\gamma=\frac{a}{1+K_{SO_2}[SO_2]_g} \quad (6)$$

where $a=(4V/S\omega)k[SiO_2]K_{SO_2}$. As shown in Figure 1C, the equation 6 can well describe the correlation of the SO_2 uptake coefficient with the SO_2 concentration, suggesting that the L-H mechanism can explain the influence of the SO_2 concentration on $\gamma_{0,\,BET}$ and $\gamma_{s,\,BET}$.

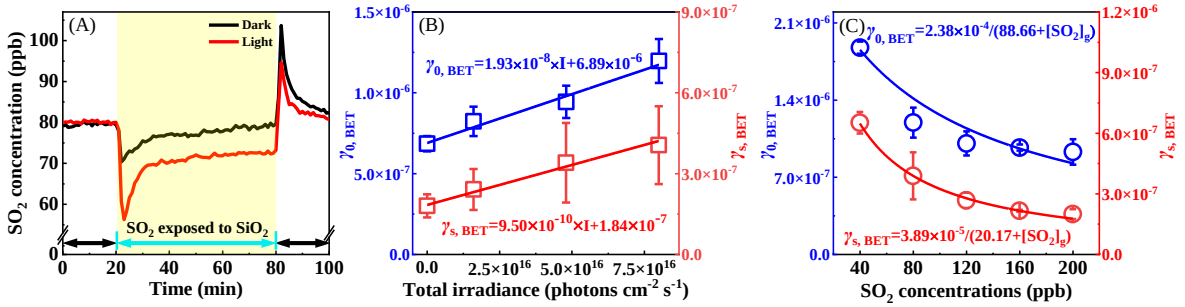

Figure 1. (A) The temporal variation of the SO_2 concentration on SiO_2 in the dark and under irradiation (7.93×10^{16} photons cm^{-2} s^{-1}); The background changes of the SO_2 concentration in the blank reactor have been deducted. (B) The $\gamma_{0,\,BET}$ and $\gamma_{s,\,BET}$ of SO_2 on SiO_2 as a function of the light intensity. (C) The $\gamma_{0,\,BET}$ and $\gamma_{s,\,BET}$ of SO_2 on SiO_2 at different SO_2 concentrations under irradiation (7.93×10^{16} photons cm^{-2} s^{-1}); The fitting lines for $\gamma_{0,\,BET}$ and $\gamma_{s,\,BET}$ were based on the Langmuir-Hinshelwood mechanism using equation 6. Reaction conditions: SiO_2 mass of 0.2 g, temperature of 298 K, RH of 40% and O_2 content of 20%.

3.2 Photo-induced formation of sulfates by the SO_2 uptake

To investigate the products formed on SiO_2, *in situ* DRIFTS spectra were recorded, as shown in Figure 2. The band at 1359 cm^{-1} was assigned to physically-adsorbed SO_2 on SiO_2 (Urupina et al., 2019). The bidentate sulfate and bisulfate contributed to the bands at 1260 and 1229/1074 cm^{-1} (Urupina et al., 2019; Yang et al., 2020), respectively. The bands at 1038 cm^{-1} may be related to the monodentate sulfite (Yang et al., 2019; Wang et al., 2019). It was noted that the intensity of physically-absorbed SO_2 (1359 cm^{-1}) under irradiation was lower than that in the dark (Figure S7), which may be ascribed to further conversion of SO_2 absorbed on SiO_2 under irradiation. Especially, the sulfate bands (1260, 1229 and 1074 cm^{-1}) only appeared under irradiation, while the sulfites (1038 cm^{-1}) were only detected in the dark. This suggests that light changed the SO_2 conversion pathways on SiO_2. As shown in Figure S7, the bands at 1157/1055 cm^{-1} were assigned to the asymmetric stretching of Si−O (Hu et al., 2003). Sulfate generated on the surface may interact with SiO_2, leading to a decrease in the intensity of peaks (1157/1055 cm^{-1}).

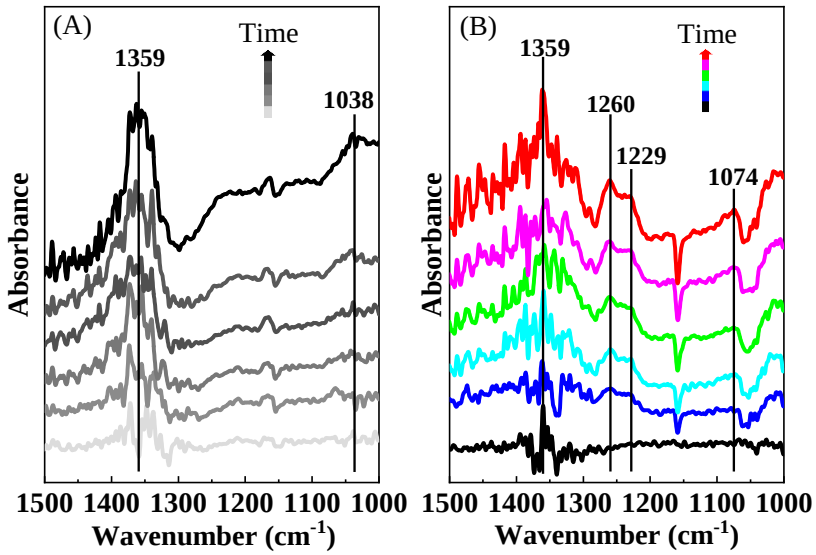

Figure 2. *In situ* DRIFTS spectra of SiO_2 during the uptake process of SO_2 (2 ppm) in the dark (A) and under irradiation (B). Reaction conditions: RH of 40%, temperature of 298 K and O_2 content of 20%.

3.3 Key roles of H_2O and O_2 in photochemical conversion of SO_2 to sulfates

Figure S8A shows temporal variations of the SO_2 concentration in the reaction with SiO_2 at RH=10% and 60% under irradiation. The uptake of SO_2 was very weak at RH=10%, whereas it was obvious at RH=60%. Moreover, H_2O markedly prolonged the time to reach the steady-state uptake of SO_2. This definitely determines that H_2O plays a distinct enhancement role in the photochemical uptake of SO_2. As shown in Figure 3A, $\gamma_{0,\,BET}$ had a continuous increase from $(1.20 \pm 0.04) \times 10^{-7}$ to $(1.54 \pm 0.07) \times 10^{-6}$ with increasing the RH in the 10%−60% range, but it decreased to $(1.05 \pm 0.09) \times 10^{-6}$ at RH=75%. The $\gamma_{s,\,BET}$ linearly depended on the RH, and linear fitting to $\gamma_{s,\,BET}$ versus RH yielded the equation $\gamma_{s,\,BET}=1.31\times10^{-8}\times RH-1.02\times10^{-7}$. Adsorbed H_2O promoted the hydration and dissociation of SO_2 (Huang et al., 2015), and it may generate reactive oxygen species (ROS) such as •OH or HO_2 radicals to oxidize SO_2 under irradiation (Li et al., 2020; Ma et al., 2019), which would lead to positive effects of RH on the SO_2 uptake. Adsorbed H_2O also occupied adsorptive and active sites on the surface, and produced the competition with SO_2. When this competitive role was dominated, the uptake of

SO_2 would be hindered.

The DRIFTS spectra of SiO_2 during the SO_2 uptake at different RHs are shown in Figure S9A. The band intensities of sulfates (1260 and 1229 cm^{-1}) at RH=60% were greatly stronger than those at RH=10%, suggesting that H_2O significantly promotes the sulfate formation. To further investigate the influence of H_2O on the sulfate formation, the integrated area of sulfates in the DRIFTS spectra (1289−1202 cm^{-1}) as a function of the time at different RHs is illustrated in Figure 3B. Sulfates exhibited a fast formation in the initial 30 min at any RH, and then they were continuously generated at a relatively slow rate. Absorptive sites for SO_2 can be blocked because of the accumulation of H_2O and products (sulfites and sulfates), resulting in the gradual deactivation of the surface. It was noted that sulfates had a more distinct formation trend with increasing the RH, revealing that H_2O can act as an important participator in the production of sulfates by the photochemical uptake of SO_2 on SiO_2.

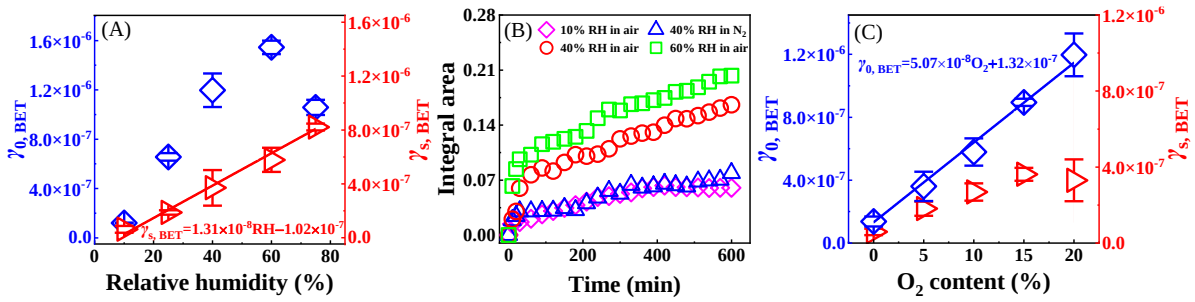

Figure 3. (A) The dependence of $\gamma_{0, BET}$ and $\gamma_{s, BET}$ on RH. (B) Integrated area of sulfates in DRIFTS spectra (1289−1202 cm^{-1}) as a function of time. (C) The dependence of $\gamma_{0, BET}$ and $\gamma_{s, BET}$ on O_2. Reaction conditions: SiO_2 mass of 0.2 g, irradiation intensity of 7.93 × 10^{16} photons cm^{-2} s^{-1}, temperature of 298 K, O_2 content of 20% for (A) and RH of 40% for (B).

Figure S8B displays effects of O_2 on the photochemical uptake of SO_2 on SiO_2. Negligible SO_2 uptake occurred in N_2, while there was a significant decrease in the SO_2 concentration in air. The $\gamma_{0, BET}$ greatly increased from (1.37 ± 0.45) × 10^{-7} in N_2 to (1.19 ± 0.13) × 10^{-6} in 20% O_2 (Figure 3C), confirming that O_2 was involved in the reaction of SO_2 on SiO_2. The $\gamma_{s, BET}$

displayed different dependence behaviors on O_2. It exhibited an increase from (7.10 ± 2.85) × 10^{-8} in N_2 to (4.37 ± 0.58) × 10^{-7} in 15% O_2, whereas it remained unchanged in 20% O_2.

DRIFTS spectra of SiO_2 during the SO_2 uptake in N_2 and air was compared in Figure S9B. In both air and N_2, the bands of absorbed SO_2 (1359 cm^{-1}), sulfates (1260, 1229 and 1074 cm^{-1}). Nevertheless, their intensities in N_2 were weaker than those in air. According to the integrated area of sulfates in the DRIFTS spectra (1289−1202 cm^{-1}) as a function of time, the formation trends of sulfates were similar in N_2 and air (Figure 3B), while the sulfate formation rate in N_2 was obviously lower than that in air, meaning that O_2 enhanced the sulfate production. It was reported that the production rate of sulfates from the SO_2 uptake on TiO_2 and by the photolysis of nitrates under UV irradiation in N_2 was also smaller than that in air (Ma et al., 2019; Gen et al., 2019b). In addition, it was noted that sulfates can be generated in N_2, meaning that O_2 was not necessary and some pathways contributed to sulfates without O_2.

3.4 Ubiquitously photoenhanced conversion of SO_2 to sulfates

To better assess the potential for photochemical conversion of SO_2 to sulfates, the SO_2 uptake experiments were further performed for typical mineral oxides without photocatalytic activity. As displayed in Figure S10, more obvious uptake behaviors of SO_2 on kaolinite, Al_2O_3, MgO and CaO were observed under irradiation when compared to those in the dark. Figure 4A shows that there was the largest $\gamma_{s,\,BET}$ for CaO among five minerals, and $\gamma_{s,\,BET}$ positively depended on the basicity (pH) of mineral oxides. Basic oxides generally contains more surface hydroxyls, which is in favor of sulfite and sulfate formation to enhance the heterogeneous uptake of SO_2 (Zhang et al., 2006). The ratios of steady-state uptake coefficients under irradiation to those in the dark ($\gamma_{s,\,Light}/\gamma_{s,\,Dark}$) were larger than 1.0 for all mineral oxides (Figure 4B). The experiments for the pH dependence on SiO_2 have been also performed (Figure S11). The pH of SiO_2 suspension was adjusted to pH = 9, and $\gamma_{s,\,BET}$ and $\gamma_{s,\,Light}/\gamma_{s,\,Dark}$ were determined to be (8.79 ± 0.85) × 10^{-6} and 1.31, respectively. These results suggest that light can generally enhance the SO_2 uptake on minerals at a wide pH range. However, the $\gamma_{Light}/\gamma_{Dark}$ had smaller values with an increase in the basicity, suggesting that the promotion effect of the light was less

remarkable for basic oxides.

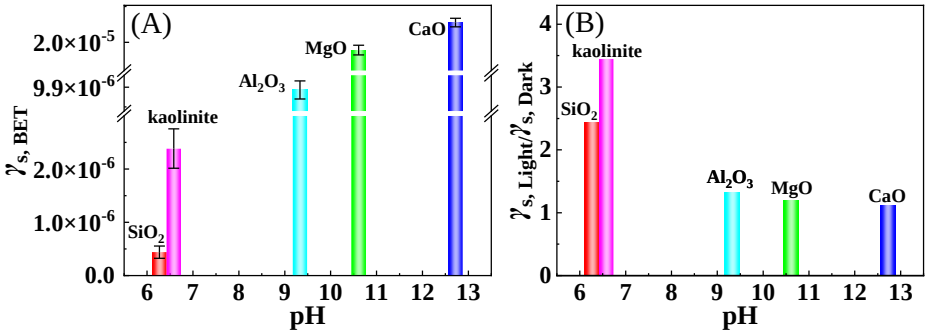

Figure 4. (A) The dependence of $\gamma_{s,\,BET}$ under irradiation on the basicity (pH) of mineral oxides. (B) The ratios of steady-state uptake coefficients under irradiation to those in the dark ($\gamma_{s,\,Light}/\gamma_{s,\,Dark}$). Reaction conditions: mineral oxides mass of 0.2 g, irradiation intensity of 7.93×10^{16} photons cm^{-2} s^{-1}, temperature of 298 K, RH of 40% and O_2 content of 20%.

As shown in Figure 5A and B, the band at 1300 cm^{-1} should be ascribed to the sulfate. The intensity of sulfate (1300 and 1220 cm^{-1}) under irradiation was larger than those in the dark. Compared to weaker peaks of sulfates (1200 and 1260 cm^{-1}) for Al_2O_3 in the dark (Figure 5C), a stronger band of bisulfates appeared at 1220 cm^{-1} under irradiation (Figure 5D). By contrast to the generation of sulfates for kaolinite and Al_2O_3, both sulfites and sulfates formations were observed for MgO and CaO (Figure 5E–H). Sulfites were dominant in the dark, as shown by the peaks at 966 and 1020 cm^{-1} for MgO and 943 cm^{-1} for CaO, whereas the sulfate formation was significantly enhanced under irradiation according to peak intensities at 1163 cm^{-1} for MgO and 1137 cm^{-1} for CaO. It should be noted that these mineral oxides were non-photoactive because of their poor light absorption property (Figure S1). Nevertheless, it was very surprised that the light can greatly promote the formation of sulfates via the SO_2 uptake process on mineral oxides without photocatalytic activity, which was strongly suggested to be a new and important finding for atmospheric sulfate sources.

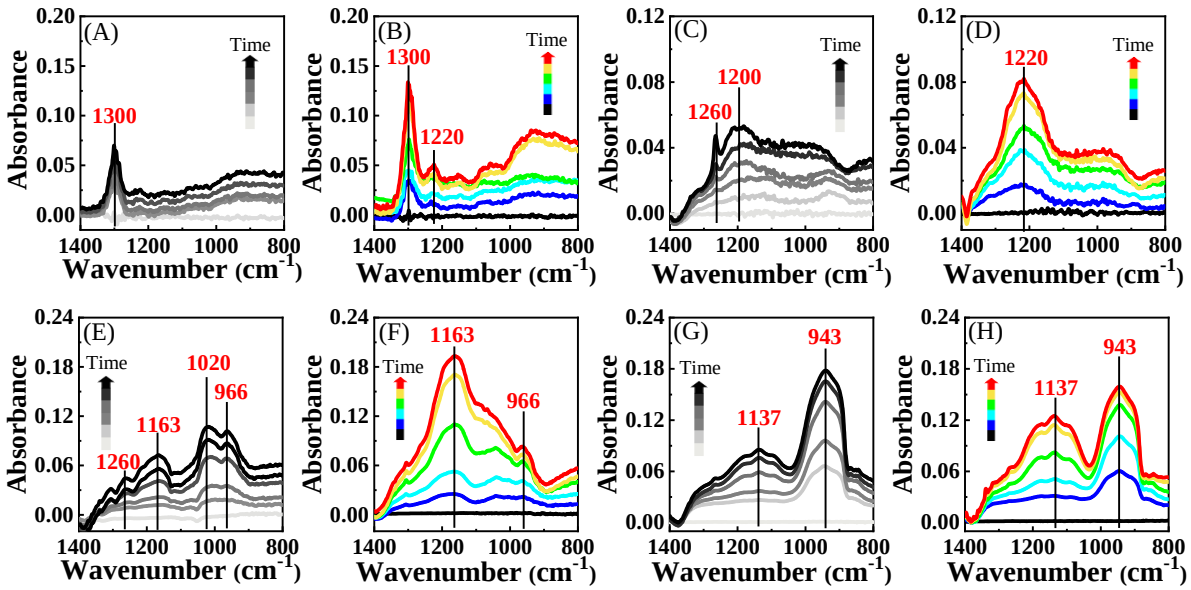

Figure 5. *In situ* DRIFTS spectra of kaolinite (A and B), Al_2O_3 (C and D), MgO (E and F), CaO (G and H) during the uptake process of SO_2 (2 ppm) for 600 min in the dark (black lines) and under irradiation (colorful lines). Reaction conditions: RH of 40%, temperature of 298 K and O_2 content of 20%.

3.5 Conversion mechanisms of SO_2 to sulfates

Heterogeneous photochemical reaction mechanisms of SO_2 on non-photoactive mineral dust were proposed in light of experimental observations (Figure 6). Gaseous SO_2 was adsorbed on the surface (R1), and then reacted with H_2O to form sulfites (R2). Under irradiation, adsorbed SO_2 accepted photons to form its singlet states ($^1SO_2$) and $^3SO_2$ (R3−5) (Sidebottom et al., 1972; Martins-Costa et al., 2018). The reaction between $^3SO_2$ and H_2O resulted in the formation of HOSO• and •OH (R6), which can combine with SO_2 to produce $HOSO_2$• (R7). HOSO• and $HOSO_2$• can be transformed into SO_3, which reacted with H_2O to drive the sulfate formation (R8 and R9). The interaction between $^3SO_2$ and O_2 may also generate SO_3 directly, which would be converted to sulfates subsequently (R10). Theoretical calculations suggested that the multistep reactions between $^3SO_2$ with H_2O and O_2 had small energy barriers or were barrier-free (Gong et al., 2022), which could enhance the generation of ROS and the transformation of S(IV) to S(VI). As displayed by R11 and R12, SO_2 and H_2SO_3 adsorbed on the surface may be oxidized to form sulfates via the reactions with ROS including •O, •OH or HO_2• , which were

produced in R6 and R8−10. In addition, gaseous SO_2 could be dissolved into adsorbed H_2O to generate bisulfites, which would be finally converted to sulfates by ROS (R13) (Urupina et al., 2019). As displayed in Figure S12A, the IR peaks of sulfates were not observed when tris (2,2′-bipyridine) ruthenium dihydrochloride ($Ru(bpy)_3(Cl)_2$) was employed as the quencher of $^3SO_2$. The peaks were assigned to the vibrations of excited $Ru(bpy)_3(Cl)_2$ (Mukuta et al., 2014). This definitely proves that $^3SO_2$ is the key trigger for the sulfate formation. Figure S12B shows that the peaks of sulfates were obviously weaker in the presence of $NaHCO_3$, confirming the dominant contribution of •OH formed in R6 and R9 to the formation of sulfates.

Several photochemical mechanisms have been reported to explain the sulfate formation via the SO_2 uptake on various surfaces. Photoactive mineral oxides (such as TiO_2, F_2O_3 and ZnO) can accept photons to produce electron-hole pairs, which generated ROS for the conversion of SO_2 to sulfates (Ma et al., 2019; Li et al., 2019; Wang et al., 2020b). For example, •OH and HO_2•, generated from the reaction of hole with H_2O and electron with O_2, respectively, can act as oxidizing agents for the reaction with SO_2 (Ma et al., 2019). Similarly, the reaction of SO_2 with photo-induced •OH obviously enhanced the formation of sulfate on diesel soot and actual $PM_{2.5}$ (Zhang et al., 2022; Zhang et al., 2020c). NO_2 and NO_2^-/HNO_2 can be formed in the nitrates photolysis, and primarily contributed to the oxidation of SO_2 to sulfates on nitrates (Gen et al., 2019b; Gen et al., 2019a). Theoretically, the mechanism proposed in this study should also occur on photo-excited substrates. Taking TiO_2 as an example, SO_2 competed with TiO_2 for photons, and the production efficiency of $^3SO_2$ and excited state of TiO_2 (TiO_2*) depended on their light absorption properties. Meanwhile, $^3SO_2$ had a competition electron-hole pairs generated from TiO_2* for O_2 and H_2O. Thus, the dominant mechanism for the SO_2 uptake on TiO_2 should be related to light absorption properties of precursors and the reactivity for $^3SO_2$ and TiO_2* to O_2 and H_2O. By contrast, all mineral oxides used here cannot be excited under irradiation according to their light absorption spectra (Figure S1). Nevertheless, SO_2 adsorbed on mineral oxides can absorb the ultraviolet radiation (290−400 nm) to form the excited states of SO_2 (SO_2^*) (Kroll et al., 2018), which subsequently reacted with H_2O and O_2, finally converting SO_2 to sulfates. The SO_2 uptake experiment in the dark and the visible light (>420

nm) was carried out (Figure S13). An ignorable difference was observed for the SO_2 concentration with or without visible light, suggesting that visible light had a minor contribution to the photoenhanced SO_2 uptake.

According to the experimental results, some surfaces, providing absorptive sites for SO_2, can enhance the photooxidation of SO_2 to sulfates. However, the promotion effect would vary with different substances. For example, the current experiments on some basic minerals indicate that light plays a minor enhancement role in the SO_2 uptake (Figure 4), but it could still enhance the sulfate formation (Figure 5). The solubility and effective Henry's law constant of SO_2 were positively dependent on pH. Thus, SO_2 was more liable to be dissolved to form HSO_3^-/SO_3^{2-} on more alkaline surface, leading to a strong SO_2 uptake in the dark (Figure 4A and 4B), and abundant sulfites on surfaces (Figure 5). Nevertheless, gaseous SO_2 tends to be adsorbed on kaolinite and Al_2O_3 due to less solubility of SO_2 on these surfaces, and then converted to sulfate under irradiation (Figure 6). Accordingly, a strong promotion effect of light on SO_2 uptake was observed on neutral and weakly alkaline surfaces (Figure 4B).

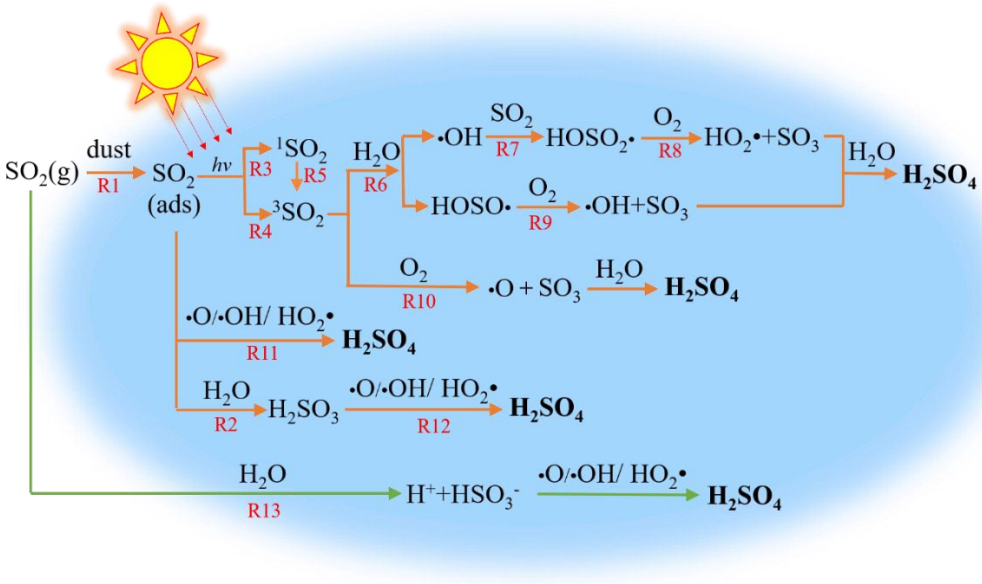

Figure 6. The proposed photochemical conversion mechanisms of SO_2 to sulfates on non-photoactive mineral dust.

4 Atmospheric implications

The lifetime (τ) for photochemical loss of SO_2 on mineral dust was given using the equation

7,

$$\tau = \frac{4}{\gamma \omega A} \quad (7)$$

where γ and ω are the uptake coefficient and the mean molecular speed of SO_2, respectively; A is the surface area density of mineral dust, and it is estimated to be (1.4–4.8) × 10^{-5} cm^2 cm^{-3} (Zhang et al.,2019; He et al., 2018b). In this work, $\gamma_{s,\,BET}$ of SO_2 on several mineral oxides were measured to be from 4.39 × 10^{-7} to 3.45 × 10^{-5} under conditions with SO_2 concentration of 40 ppb, irradiation intensity of 7.93 × 10^{16} photons cm^{-2} s^{-1} and RH of 40%. Thus, the τ of SO_2 with respect to the photooxidation on mineral dust was calculated to be 0.9–240 days, which was shorter than that (54 years) for the photochemical uptake of SO_2 on TiO_2 and the corresponding one (346 days) for the heterogeneous oxidation of SO_2 on ATD in the presence of nitrates (Ma et al., 2019; Zhang et al., 2019). The reaction conditions in this study and those in the literatures are different in some respects, and the previously reported SO_2 uptake coefficient (10^{-7}–10^{-6}) had a lower value (Ma et al., 2019). The huge difference in the τ of SO_2 was also ascribed to the variation in the surface area density. The content of TiO_2 in mineral dust was only about 1%, and thus the surface area density of TiO_2 was about 10^{-7} cm^2 cm^{-3}, leading to a longer τ (54 years) for SO_2 on TiO_2 (Ma et al., 2019). It was comparable to the lifetime (3.6–20 days) of SO_2 for the gas-phase reaction with •OH at a concentration of ~10^{-6} molecules cm^{-3} (Huang et al., 2015; Zhang et al., 2019). Therefore, the photochemical process with the excited state SO_2 acting as a driver on mineral dust was an important pathway for the SO_2 sink in the atmosphere.

Sulfates show significant influences on the atmosphere, such as an important contributor to the haze formation, affecting the activity of aerosols acting as cloud condensation nuclei (CCN) and ice nuclei (IN), and modifying optical property and acidity of aerosols. A sulfate formation rate (R) can be obtained using γ by the equation 8 (Cheng et al., 2016),

$$R = \frac{d\left[SO_4^{2-}\right]}{dt} = \left[\frac{R_p}{D} + \frac{4}{\gamma \omega}\right]^{-1} A\left[SO_2\right] \quad (8)$$

where R_P is the radius of mineral dust, which can be estimated using the equation 9 (Li et al.,

2020),

$R_P = (0.254 \times [PM_{2.5}]/(\mu g\ m^{-3}) + 10.259) \times 10^{-9}\ m$ (9)

where $[PM_{2.5}]$ was average $PM_{2.5}$ mass concentration, and 300 $\mu g\ m^{-3}$ was used for the polluted periods in typical China cities (Li et al., 2020; Guo et al., 2014). It was assumed that mineral dust accounted for 50% mass of $PM_{2.5}$ (Tohidi et al., 2022), and the mass fraction of SiO_2, Al_2O_3, MgO, and CaO in mineral dust was 60%, 12.5%, 4% and 6.5%, respectively (Urupina et al., 2021; Urupina et al., 2019; Usher et al., 2003). Thus, R was determined to be 2.15 $\mu g\ m^{-3}\ h^{-1}$. This suggests that the SO_2 on non-photoactive surfaces is a newly identified sulfate formation pathway in some dust-rich conditions.

Author contributions

CH, WY and JM designed and conducted experiments; CH, WY and JM analyzed the data and prepared the paper with contributions from HY; FL conducted experiments; CH supervised the project.

Competing interests

The authors declare that they have no conflict of interest.

Acknowledgements

This work was supported by the National Natural Science Foundation of China [grant number 42077198], the LiaoNing Revitalization Talents Program [grant number XLYC1907185], and the Fundamental Research Funds for the Central Universities [grant numbers N2325034; N2025011].

Reference

Adams, J., Rodriguez, D., and Cox, R.: The uptake of SO_2 on Saharan dust: A flow tube study, Atmos. Chem. Phys., 5, 2679-2689, https://doi.org/10.5194/acpd-5-2643-2005, 2005.

Alexander, B., Park, R. J., Jacob, D. J., and Gong, S.: Transition metal-catalyzed oxidation of atmospheric sulfur: Global implications for the sulfur budget, J. Geophy. Res., 114, 2309-

2312, https://doi.org/10.1029/2008jd010486, 2009.
Ammann, M., Poschl, U., and Rudich, Y.: Effects of reversible adsorption and Langmuir-Hinshelwood surface reactions on gas uptake by atmospheric particles, Phys. Chem. Chem. Phys., 5, 351-356, https://doi.org/10.1039/b208708a, 2003.
Bounechada, D., Anderson, D., Skoglundh, M., and Carlsson, P.: SO_2 adsorption on silica supported iridium, J. Chem. Phys., 146, 084701-084708, https://doi.org/10.1063/1.4976835, 2017.
Brunauer, B., Deming, L., Deming, W., and Teller, E.: Adsorption of gases in multimolecular layers, J. Am. Chem. Soc., 60, 309-319, https://doi.org/10.1021/ja01269a023, 1938.
Bulgakov, R. G. and Safonova, L. A.: Chemiluuminescence in the oxidation of Na_2S by oxygen in water solutions, Russ. Chem. Bull., 45, 1775-1776, https://doi.org/10.1007/bf01431827, 1996.
Cao, J., Tie, X., Dabberdt, W. F., Jie, T., Zhao, Z., An, Z., Shen, Z., and Feng, Y.: On the potential high acid deposition in northeastern China, J. Geophy. Res.: Atmos., 118, 4834-4846, https://doi.org/10.1002/jgrd.50381, 2013.
Chan, M. and Chan, C.: Hygroscopic properties of two model humic-like substances and their mixtures with inorganics of atmospheric importance, Environ. Sci. Technol. , 37, 5109-5115, https://doi.org/10.1021/es034272o, 2003.
Chen, Y., Tong, S., Li, W., Liu, Y., Tan, F., Ge, M., Xie, X., and Sun, J.: Photocatalytic oxidation of SO_2 by TiO_2: Aerosol formation and the key role of gaseous reactive oxygen species, Environ. Sci. Technol., 55, 9784-9793, https://doi.org/10.1021/acs.est.1c01608, 2021.
Cheng, Y., Zheng, G., Wei, C., Mu, Q., Zheng, B., Wang, Z., Gao, M., Zhang, Q., He, K., Carmichael, G., Pöschl, U., and Su, H.: Reactive nitrogen chemistry in aerosol water as a source of sulfate during haze events in China, Sci. Adv., 2, 1601530-1601540, https://doi.org/10.1126/sciadv.1601530, 2016.
Chu, B., Wang, Y. L., Yang, W. W., Ma, J. Z., Ma, Q. X., Zhang, P., Liu, Y. C., and He, H.: Effects of NO_2 and C_3H_6 on the heterogeneous oxidation of SO_2 on TiO_2 in the presence or absence of UV-Vis irradiation, Atmos. Chem. Phys., 19, 14777-14790, https://doi.org/10.5194/acp-19-14777-2019, 2019.
Davis, D. D., Ravishankara, A. R., and Fischer, S.: SO_2 oxidation via the hydroxyl radical: Atmospheric fate of HSO_x radicals, Geo. Res. Lett., 6, 113-116, https://doi.org/10.1029/GL006i002p00113, 1979.
Dentener, F., Carmichael, G., Zhang, Y., Lelieveld, J., and Crutzen, P.: Role of mineral aerosol as a reactive surface in the global troposphere, J. Geophy. Res.: Atmos., 101, 22869-22889, https://doi.org/10.1029/96jd01818, 1996.
Gen, M., Zhang, R., Huang, D., Li, Y., and Chan, C.: Heterogeneous oxidation of SO_2 in sulfate production during nitrate photolysis at 300 nm: Effect of pH, relative humidity, irradiation intensity, and the presence of organic compounds, Environ. Sci. Technol., 53, 8757-8766, https://doi.org/10.1021/acs.est.9b01623, 2019a.
Gen, M., Zhang, R., Huang, D., Li, Y., and Chan, C.: Heterogeneous SO_2 oxidation in sulfate formation by photolysis of particulate nitrate, Environ. Sci. Tech. Lett., 6, 86-91, https://doi.org/10.1021/acs.estlett.8b00681, 2019b.

514 Golobokova, L., Khodzher, T., Khuriganova, O., Marinayte, I., Onishchuk, N., Rusanova, P.,
515 and Potemkin, V.: Variability of chemical properties of the atmospheric aerosol above lake
516 baikal during large wildfires in siberia, Atmosphere, 11, 1230-1250,
517 https://doi.org/10.3390/atmos11111230, 2020.
518 Gong, C., Yuan, X., Xing, D., Zhang, D., Martins-Costa, M. T. C., Anglada, J. M., Ruiz-Lopez,
519 M. F., Francisco, J. S., and Zhang, X.: Fast sulfate formation initiated by the spin-forbidden
520 excitation of SO_2 at the air-water interface, J. Am. Chem. Soc., 144, 22302-22308,
521 https://doi.org/10.1021/jacs.2c10830, 2022.
522 Goodman, A., Li, P., Usher, C., and Grassian, V.: Heterogeneous uptake of sulfur dioxide on
523 aluminum and magnesium oxide particles, J. Phys. Chem. A 105, 6109-6120,
524 https://doi.org/10.1021/jp004423z, 2001.
525 Guo, S., Hu, M., Zamora, M. L., Peng, J., Shang, D., Zheng, J., Du, Z., Wu, Z., Shao, M., Zeng,
526 L., Molina, M. J., and Zhang, R.: Elucidating severe urban haze formation in China, Proc.
527 Natl. Acad. Sci. U. S. A., 111, 17373-17378, https://doi.org/10.1073/pnas.1419604111,
528 2014.
529 Harris, E., Sinha, B., van Pinxteren, D., Tilgner, A., Fomba, K. W., Schneider, J., Roth, A.,
530 Gnauk, T., Fahlbusch, B., Mertes, S., Lee, T., Collett, J., Foley, S., Borrmann, S., Hoppe, P.,
531 and Herrmann, H.: Enhanced role of transition metal ion catalysis during in-cloud oxidation
532 of SO_2, Science, 340, 727-730, https://doi.org/10.1126/science.1230911, 2013.
533 He, G., Ma, J., and He, H.: Role of carbonaceous aerosols in catalyzing sulfate formation, ACS
534 Catal., 8, 3825-3832, https://doi.org/10.1021/acscatal.7b04195, 2018a.
535 He, H., Li, C., Loughner, C. P., Li, Z., Krotkov, N. A., Yang, K., Wang, L., Zheng, Y., Bao, X.,
536 Zhao, G., and Dickerson, R. R.: SO_2 over central China: Measurements, numerical
537 simulations and the tropospheric sulfur budget, J. Geophy. Res.: Atmos., 117, 37-51,
538 https://doi.org/10.1029/2011jd016473, 2012.
539 He, P., Alexander, B., Geng, L., Chi, X., Fan, S., Zhan, H., Kang, H., Zheng, G., Cheng, Y., Su,
540 H., Liu, C., and Xie, Z.: Isotopic constraints on heterogeneous sulfate production in Beijing
541 haze, Atmos. Chem. Phys., 18, 5515-5528, https://doi.org/10.5194/acp-18-5515-2018,
542 2018b.
543 Herrmann, H., Ervens, B., Jacobi, H. W., Wolke, R., Nowacki, P., and Zellner, R.: $CAPRAM_{2.3}$:
544 A chemical aqueous phase radical mechanism for tropospheric chemistry, J. Atmos. Chem.,
545 36, 231-284, https://doi.org/10.1023/A:1006318622743, 2000.
546 Huang, L., Zhao, Y., Li, H., and Chen, Z.: Kinetics of heterogeneous reaction of sulfur dioxide
547 on authentic mineral dust: Effects of relative humidity and hydrogen peroxide, Environ. Sci.
548 Technol., 49, 10797-10805, https://doi.org/10.1021/acs.est.5b03930, 2015.
549 Hu, Q., Suzuki, H., Gao, H., Araki, H., Yang, W., and Noda, T.: High-frequency FTIR
550 absorption of SiO_2/Si nanowires, Chem. Phys. Lett., 378, 299-304,
551 https://doi.org/10.1016/j.cplett.2003.07.015, 2003.
552 Knopf, D., Cosman, L., Mousavi, P., Mokamati, S., and Bertram, A.: A novel flow reactor for
553 studying reactions on liquid surfaces coated by organic monolayers: Methods, validation,
554 and initial results, J. Phys. Chem. A, 111, 11021-11032, https://doi.org/10.1021/jp075724c,
555 2007.

Kroll, J., Frandsen, B., Kjaergaard, H., and Vaida, V.: Atmospheric hydroxyl radical source: Reaction of triplet SO_2 and water, J. Phys. Chem. A, 122, 4465-4469, https://doi.org/10.1021/acs.jpca.8b03524, 2018.

Langhammer, D., Kullgren, J., and Osterlund, L.: Photoinduced adsorption and oxidation of SO_2 on anatase TiO_2, J. Am. Chem. Soc., 142, 21767-21774, https://doi.org/10.1021/jacs.0c09683, 2020.

Li, G., Bei, N., Cao, J., Huang, R., Wu, J., Feng, T., Wang, Y., Liu, S., Zhang, Q., Tie, X., and Molina, L. T.: A possible pathway for rapid growth of sulfate during haze days in China, Atmos. Chem. Phys., 17, 3301-3316, https://doi.org/10.5194/acp-17-3301-2017, 2017.

Li, J., Zhang, Y. L., Cao, F., Zhang, W., Fan, M., Lee, X., and Michalski, G.: Stable sulfur isotopes revealed a major role of transition-metal ion-catalyzed SO_2 oxidation in haze episodes, Environ. Sci. Technol., 54, 2626-2634, https://doi.org/10.1021/acs.est.9b07150, 2020.

Li, K., Kong, L., Zhanzakova, A., Tong, S., Shen, J., Wang, T., Chen, L., Li, Q., Fu, H., and Zhang, L.: Heterogeneous conversion of SO_2 on nano α-Fe_2O_3: the effects of morphology, light illumination and relative humidity, Environ. Sci.: Nano, 6, 1838-1851, https://doi.org/10.1039/c9en00097f, 2019.

Lim, S., Lee, M., Kim, S., and Laj, P.: Sulfate alters aerosol absorption properties in East Asian outflow, Sci. Rep., 8, 5172-5178, https://doi.org/10.1038/s41598-018-23021-1, 2018.

Liu, T., Clegg, S., and Abbatt, J. P. D.: Fast oxidation of sulfur dioxide by hydrogen peroxide in deliquesced aerosol particles, Proc. Natl. Acad. Sci. U. S. A., 117, 1354-1359, https://doi.org/10.1073/pnas.1916401117, 2020a.

Liu, T., Chan, A. W. H., and Abbatt, J. P. D.: Multiphase oxidation of sulfur dioxide in aerosol particles: Implications for sulfate formation in polluted environments, Environ. Sci. Technol., 55, 4227-4242, https://doi.org/10.1021/acs.est.0c06496, 2021.

Liu, Y., Deng, Y., Liu, J., Fang, X., Wang, T., Li, K., Gong, K., Bacha, A. U., Nabi, I., Ge, Q., Zhang, X., George, C., and Zhang, L.: A novel pathway of atmospheric sulfate formation through carbonate radicals, Atmos. Chem. Phys., 22, 9175-9197, https://doi.org/10.5194/acp-22-9175-2022, 2022.

Ma, J., Dörner, S., Donner, S., Jin, J. L., Cheng, S. Y., Guo, J. R., Zhang, Z. F., Wang, J. Q., Liu, P., Zhang, G. Q., Pukite, J., Lampel, J., and Wagner, T.: MAX-DOAS measurements of NO_2, SO_2, HCHO, and BrO at the Mt. Waliguan WMO GAW global baseline station in the Tibetan Plateau, Atmos. Chem. Phys., 20, 6973-6990, https://doi.org/10.5194/acp-20-6973-2020, 2020.

Ma, Q., Wang, L., Chu, B., Ma, J., and He, H.: Contrary role of H_2O and O_2 in the kinetics of heterogeneous photochemical reactions of SO_2 on TiO_2, J. Phys. Chem. A., 123, 1311-1318, https://doi.org/10.1021/acs.jpca.8b11433, 2019.

Martins-Costa, M., Anglada, J., Francisco, J., and Ruiz-Lopez, M.: Photochemistry of SO_2 at the air-water interface: A source of OH and HOSO radicals, J. Am. Chem. Soc., 140, 12341-12344, https://doi.org/10.1021/jacs.8b07845, 2018.

Mauldin, R., Berndt, T., Sipila, M., Paasonen, P., Petaja, T., Kim, S., Kurten, T., Stratmann, F., Kerminen, V., and Kulmala, M.: A new atmospherically relevant oxidant of sulphur dioxide,

Nature, 488, 193-196, https://doi.org/10.1038/nature11278, 2012.
Mukuta, T., Fukazawa, N., Murata, K., Inagaki, A., Akita, M., Tanaka, S., Koshihara, S. Y., and Onda, K.: Infrared vibrational spectroscopy of $[Ru(bpy)_2(bpm)]^{2+}$ and $[Ru(bpy)_3]^{2+}$ in the excited triplet state, Inorg. Chem., 53, 2481-2490, https://doi.org/10.1021/ic402474t, 2014.
Olson, E., Michalski, G., Welp, L., Valdivia, A., Larico, J., Pen, J., Fang, H., Gomez, K., and Li, J.: Mineral dust and fossil fuel combustion dominate sources of aerosol sulfate in urban Peru identified by sulfur stable isotopes and water-soluble ions, Atmos. Environ., 260, 118482-118495, https://doi.org/10.1016/j.atmosenv.2021.118482, 2021.
Park, J. and Jang, M.: Heterogeneous photooxidation of sulfur dioxide in the presence of airborne mineral dust particles, RSC Adv., 6, 58617-58627, https://doi.org/10.1039/c6ra09601h, 2016.
Park, J., Jang, M., and Yu, Z.: Heterogeneous photo-oxidation of SO_2 in the presence of two different mineral dust particles: Gobi and arizona dust, Environ. Sci. Technol., 51, 9605-9613, https://doi.org/10.1021/acs.est.7b00588, 2017.
Peng, Y., von Salzen, K., and Li, J.: Simulation of mineral dust aerosol with Piecewise Log-normal Approximation (PLA) in CanAM4-PAM, Atmos. Chem. Phys., 12, 6891-6914, https://doi.org/10.5194/acp-12-6891-2012, 2012.
Prospero, J.: Long-range transport of mineral dust in the global atmosphere: Impact of African dust on the environment of the southeastern United States, Proc. Natl. Acad. Sci. U. S. A., 96, 3396-3403, https://doi.org/10.1073/pnas.96.7.3396, 1999.
Shao, J., Chen, Q., Wang, Y., Lu, X., He, P., Sun, Y., Shah, V., Martin, R. V., Philip, S., Song, S., Zhao, Y., Xie, Z., Zhang, L., and Alexander, B.: Heterogeneous sulfate aerosol formation mechanisms during wintertime Chinese haze events: air quality model assessment using observations of sulfate oxygen isotopes in Beijing, Atmos. Chem. Phys., 19, 6107-6123, https://doi.org/10.5194/acp-19-6107-2019, 2019.
Shiraiwa, M., Ueda, K., Pozzer, A., Lammel, G., Kampf, C. J., Fushimi, A., Enami, S., Arangio, A. M., Frohlich-Nowoisky, J., Fujitani, Y., Furuyama, A., Lakey, P. S. J., Lelieveld, J., Lucas, K., Morino, Y., Poschl, U., Takahama, S., Takami, A., Tong, H., Weber, B., Yoshino, A., and Sato, K.: Aerosol health effects from molecular to global scales, Environ. Sci. Technol., 51, 13545-13567, https://doi.org/10.1021/acs.est.7b04417, 2017.
Sidebottom, H. W., Badcock, C. C., Jackson, G. E., Calvert, J. G., Reinhardt, G. W., and Damon, E. K.: Photooxidation of sulfur dioxide, Environ. Sci. Technol., 6, 72-79, https://doi.org/10.1080/00022470.1971.10469552, 1972.
Solbrig, C. W. and Gidaspow, D.: Convective diffusion in a parallel plate duct with one catalytic wall, laminar flow, first order reaction-part one, Can. J. Chem. Eng., 45, 35-39, https://doi.org/10.1016/0304-5102(89)80197-X, 1967.
Sumner, A. L., Menke, E. J., Dubowski, Y., Newberg, J. T., Penner, R. M., Hemminger, J. C., Wingen, L. M., Brauers, T. and Finlayson-Pitts, B. J. The nature of water on surfaces of laboratory systems and implications for heterogeneous chemistry in the troposphere. Phys. Chem. Chem. Phys., 6, 604-613, https://doi.org/10.1039/B308125G, 2004.
Tohidi, R., Farahani, V., and Sioutas, C.: Real-time measurements of mineral dust concentration in coarse particulate matter $PM_{10-2.5}$ by employing a novel optical-based technique in Los

Angeles, Sci. Total. Environ., 838, 156215-156226, https://doi.org/10.1016/j.scitotenv.2022.156215, 2022.
Urupina, D., Romanias, M. N., and Thevenet, F.: How relevant is it to use mineral proxies to mimic the atmospheric reactivity of natural dust samples? A reactivity study using SO_2 as probe molecule, Minerals, 11, 282-299, https://doi.org/10.3390/min11030282, 2021.
Urupina, D., Lasne, J., Romanias, M. N., Thiery, V., Dagsson-Waldhauserova, P., and Thevenet, F.: Uptake and surface chemistry of SO_2 on natural volcanic dusts, Atmos. Environ., 217, 116942-116959, https://doi.org/10.1016/j.atmosenv.2019.116942, 2019.
Usher, C., Michel, A., and Grassian, V.: Reactions on mineral dust, Chem. Rev. , 103, 4883-4939, https://doi.org/10.1021/cr020657y, 2003.
Usher, C., Al-Hosney, H., Carlos-Cuellar, S., and Grassian, V.: A laboratory study of the heterogeneous uptake and oxidation of sulfur dioxide on mineral dust particles, J. Geophys. Res-atmos. , 107, 4713-4729, https://doi.org/10.1029/2002jd002051, 2002.
Wang, J., Li, J., Ye, J., Zhao, J., Wu, Y., Hu, J., Liu, D., Nie, D., Shen, F., Huang, X., Huang, D. D., Ji, D., Sun, X., Xu, W., Guo, J., Song, S., Qin, Y., Liu, P., Turner, J. R., Lee, H. C., Hwang, S., Liao, H., Martin, S. T., Zhang, Q., Chen, M., Sun, Y., Ge, X., and Jacob, D. J.: Fast sulfate formation from oxidation of SO_2 by NO_2 and HONO observed in Beijing haze, Nat. Commun., 11, 2844-2850, https://doi.org/10.1038/s41467-020-16683-x, 2020a.
Yao, M., Zhao, Y., Hu, M., Huang, D., Wang, Y., Yu, J. Z., and Yan, N.: Multiphase reactions between secondary organic aerosol and sulfur dioxide: Kinetics and contributions to sulfate formation and aerosol aging. Environ. Sci. Technol. Lett., 6, 768-774, https://doi.org/10.1021/acs.estlett.9b00657, 2019.
Ye, J., Abbatt, J. P. D., Chan, A. W. H.: Novel pathway of SO_2 oxidation in the atmosphere: Reactions with monoterpene ozonolysis intermediates and secondary organic aerosol. Atmos. Chem. Phys., 18, 5549-5565, https://doi.org/10.5194/acp-18-5549-2018, 2018.
Wang, S., Zhou, S., Tao, Y., Tsui, W. G., Ye, J., Yu, J. Z., Murphy, J. G., McNeill, V. F., Abbatt, J. P. D., and Chan, A. W. H.: Organic peroxides and sulfur dioxide in aerosol: Source of particulate sulfate. Environ. Sci. Technol., 53, 10695-10704, https://doi.org/10.1021/acs.est.9b02591, 2019.
Wang, T., Liu, Y., Deng, Y., Fu, H., Zhang, L., and Chen, J.: The influence of temperature on the heterogeneous uptake of SO_2 on hematite particles, Sci. Total. Environ., 644, 1493-1502, https://doi.org/10.1016/j.scitotenv.2018.07.046, 2018.
Wang, T., Liu, Y. Y., Deng, Y., Cheng, H. Y., Yang, Y., Li, K. J., Fang, X. Z., and Zhang, L. W.: Irradiation intensity dependent heterogeneous formation of sulfate and dissolution of ZnO nanoparticles, Environ. Sci.: Nano, 7, 327-338, https://doi.org/10.1039/c9en01148j, 2020b.
Wang, Z., Wang, T., Fu, H., Zhang, L., Tang, M., George, C., Grassian, V. H., and Chen, J.: Enhanced heterogeneous uptake of sulfur dioxide on mineral particles through modification of iron speciation during simulated cloud processing, Atmos. Chem. Phys., 19, 12569-12585, https://doi.org/10.5194/acp-19-12569-2019, 2019.
Yang, N., Tsona, N. T., Cheng, S., Li, S., Xu, L., Wang, Y., Wu, L., and Du, L.: Competitive reactions of SO_2 and acetic acid on α-Al_2O_3 and $CaCO_3$ particles, Sci. Total. Environ., 699, 134362-134370, https://doi.org/10.1016/j.scitotenv.2019.134362, 2020.

Yang, W., Ma, Q., Liu, Y., Ma, J., Chu, B., and He, H.: The effect of water on the heterogeneous reactions of SO_2 and NH_3 on the surfaces of α-Fe_2O_3 and γ-Al_2O_3, Environ. Sci.: Nano, 6, 2749-2758, https://doi.org/10.1039/c9en00574a, 2019.

Zhang, P., Chen, T., Ma, Q., Chu, B., Wang, Y., Mu, Y., Yu, Y., and He, H.: Diesel soot photooxidation enhances the heterogeneous formation of H_2SO_4, Nat. Commun., 13, 5364-5372, https://doi.org/10.1038/s41467-022-33120-3, 2022.

Zhang, R., Gen, M., Huang, D., Li, Y., and Chan, C.: Enhanced sulfate production by nitrate photolysis in the presence of halide ions in atmospheric particles, Environ. Sci. Technol., 54, 3831-3839, https://doi.org/10.1021/acs.est.9b06445, 2020a.

Zhang, T., Yang, W., Han, C., Yang, H., and Xue, X.: Heterogeneous reaction of ozone with syringic acid: Uptake of O_3 and changes in the composition and optical property of syringic acid, Environ. Pollut., 257, 113632-113638, https://doi.org/10.1016/j.envpol.2019.113632, 2020b.

Zhang, X., Zhuang, G., Chen, J., Wang, Y., Wang, X., An, Z., and Zhang, P.: Heterogeneous reactions of sulfur dioxide on typical mineral particles, J. Phys. Chem. B, 110, 12588-12596, https://doi.org/10.1021/jp0617773, 2006.

Zhang, Y., Bao, F., Li, M., Chen, C., and Zhao, J.: Nitrate-enhanced oxidation of SO_2 on mineral dust: A vital role of a proton, Environ. Sci. Technol., 53, 10139-10145, https://doi.org/10.1021/acs.est.9b01921, 2019.

Zhang, Y., Bao, F., Li, M., Xia, H., Huang, D., Chen, C., and Zhao, J.: Photoinduced uptake and oxidation of SO_2 on Beijing urban $PM_{2.5}$, Environ. Sci. Technol., 54, 14868-14876, https://doi.org/10.1021/acs.est.0c01532, 2020c.